



# Topical advances in synthesis for energy-efficient magnetoplumbite nanoferrites

M. Anis-ur-Rehman<sup>1</sup>

© Springer Nature Switzerland AG 2019

## Abstract

Next-generation magnetic devices will be planar, smaller, light weight, and will do well beyond the present state-of-the-art devices. For this to become a reality, advances in ferrite materials must first be realized. Due to superior coercivity and lower material and processing cost, magnetoplumbites are preferred over the other types of hard ferrites. Magnetoplumbites are important hexagonal ferrites with formula  $RFe_{12}O_{19}$ , where R may be barium (Ba), strontium (Sr) or lead (Pb). Energy losses are important issues in these magnetic materials. Although  $SrFe_{12}O_{19}$  have many advantages, but to lower the energy losses we need to improve the resistivity by reducing eddy current losses. Sr-Ba nanoferrites have potential for next generation of energy-efficient magnetic devices. Gadolinium (Gd) belongs to the lanthanide series. In this work, Sr hexaferrites and Sr-Ba hexaferrites doped with rare earth metal like Gd were synthesized to increase their resistivity. Strontium barium hexaferrites with composition  $Sr_{1-x}Ba_xFe_{12-y}Gd_yO_{19}$  ( $x=0.0, 0.25$  and  $y=0.0, 0.20$ ) were synthesized by without water and surfactants (WOWS) sol-gel method and co-precipitation method, respectively. All the synthesized samples showed hexagonal structure with P63/mmc space group. Crystallite sizes obtained using Scherrer's formula were in nanoregime. DC electrical properties as a function of temperature and dielectric spectroscopy as a function of frequency were evaluated and are correlated with the structural properties. A comparative study of different proportions of iron oxide and Gd dopant was carried out, and composition with  $x=0.25$  and  $y=0.20$  seems to be a suitable combination for high-frequency efficient devices.

**Keywords** Hexaferrites · Structural properties · Dielectric loss · AC conductivity · Dielectric constant

## 1 Introduction

Ferrites are believed to be the widest applied materials as metal oxides. Ferrites have two main kinds, soft magnetic and hard magnetic ferrites. Soft ferrites are prepared by elementary materials which are iron oxide and other metal oxides like manganese oxide, nickel oxide, cobalt oxide and zinc oxide [1, 2]. Hard ferrites are widely used as permanent magnetic materials which are fabricated using strontium, barium and lead in oxide or nitrate form [3, 4]. Hexagonal ferrites have varied application as permanent magnets due to truncated cost, high resistivity, striking magnetic and electrical properties [5]. Characteristics of

nanomaterials are influenced by surface atoms when their size approaches nanoscale. M-type hexaferrites are highly resistive complexes having iron oxide as main constituent. Among different types of ferrites, the hexagonal ferrites have numerous applications and a vast period of production. Also, these have high coercive force, high Curie temperature and excellent chemical stability [2]. The M-type hexaferrites usually have hexagonal symmetry of space group of P63/mmc [3]. The structural and electrical behaviors of ferrites are based on factors like crystallite size, particle size, chemical composition and synthesis procedures. M-type is important class of hexagonal ferrites with formula  $RFe_{12}O_{19}$  where R may be strontium (Sr), barium (Ba)

✉ M. Anis-ur-Rehman, marehman@comsats.edu.pk | <sup>1</sup> Applied Thermal Physics Laboratory, Department of Physics, COMSATS University Islamabad, Park Road, Islamabad 45550, Pakistan.



and lead (Pb) [6]. Hexagonal ferrites have electrical and magnetic properties which are dependent on the condition in which synthesis takes place and the site occupation of substitute cation with different  $\text{Fe}^{3+}$  sublattices named as trigonal bipyramid (2b), tetrahedral (4f) and octahedral (12 k, 2a and 4f2) of hexagonal structure [6]. To enhance the properties of Sr hexaferrite and make the material useful for different applications, various scientists doped different elements and combination of various metallic cations.

Strontium and barium have reasonable magnetic properties. Barium ferrite is important for several reasons like stable crystalline features; it has high coercive force and low density and consists of ultra-fine particle with high specific magnetic energy [6]. Significance of barium strontium hexaferrites is due to holding chemical stability, high coercivity and high magnetic anisotropy. Both strontium and barium have same crystalline structure as that of magnetoplumbite. A lot of work has been done to understand the impact of various dopants for iron and barium. The consequence of frequencies on the electrical behavior can be elucidated based on charge transport phenomena [7]. The usual fabrication methods used for hexaferrites are hydrothermal techniques, co-precipitation approach and simplified or Wows sol-gel method [8, 9]. Wows sol-gel is wet chemical method (a simplified and more economic form of sol-gel method) used in the fields of material science and ceramics engineering. This is a preferable method due to simplicity, high-purity goods and can produce dense coatings to overcome corrosion. In divergence to others, co-precipitation method has gained deep attention on immense industrial production, low cost and allows to control the particle size more resourcefully [8].

Electrical properties (AC and DC) were measured at room temperature as well as with temperature using LCR meter over frequency range from 20 Hz to 3 MHz. Crystallinity, crystallite sizes and phase purity were obtained by X-ray diffraction. The main effort of this paper is to provide current information about electrical and structural properties of Sr-Ba hexaferrites.

## 2 Experimental details

The precursor chemicals used in the synthesis of samples were  $\text{Sr}(\text{NO}_3)_2$ ,  $\text{Fe}(\text{NO}_3)_3 \cdot 9\text{H}_2\text{O}$ ,  $\text{GdN}_3\text{O}_9 \cdot 6\text{H}_2\text{O}$  and  $\text{Ba}(\text{NO}_3)_2$ . All the reagents were of analytical grade and were used without any further treatment. The Sr hexaferrite samples substituted with Ba and Gd with nominal composition  $\text{Sr}_{1-x}\text{Ba}_x\text{Fe}_{12-y}\text{Gd}_y\text{O}_{19}$  ( $x=0.0, 0.25$  and  $y=0.0, 0.20$ ) were prepared by two different chemical methods. The precursors were prepared by dissolving  $\text{Sr}(\text{NO}_3)_2$ ,  $\text{GdN}_3\text{O}_9 \cdot 6\text{H}_2\text{O}$  and  $\text{Fe}(\text{NO}_3)_3 \cdot 9\text{H}_2\text{O}$  in deionized water for co-precipitation

method. Molarity for all the solutions was maintained at 0.4 M, and they were separately stirred for 20 min. After mixing the precursor solutions at room temperature, the temperature of mixture was raised to 70 °C at the rate of 10° per minute. Sodium hydroxide solution (2.0 M) was prepared by dissolving it in deionized water. This was required to control the pH (= 12) of the solution. The mixture of all was kept for constant magnetic stirring at 70 °C for 45 min. Brown precipitates were obtained after heating and stirring. The precipitates were washed by deionized water and then dried in an oven at 105 °C for overnight. For preparation of hexaferrites by Wows sol-gel, ethylene glycol was used as a gelling agent. Precursor reagents mass-to-ethylene glycol ratio was optimized at 1:14 [8, 9]. The solutions thus obtained were heated at 80 °C till the gel is formed, and then, temperature was raised to 150 °C to get the fine powder. All prepared powder samples were calcined at 910 °C for 20 min. Calcined powders were pressed into pellets of diameter 13 mm and were sintered at 920 °C for 20 min.

## 3 Results and discussion

### 3.1 X-ray diffraction analysis

X-ray diffraction (XRD) is the useful method for obtaining the insight of structure. Figure 1 shows the XRD pattern of all the samples. The hexaferrites formation with space group P63/mmc is confirmed. Maximum intensity peaks were observed (ICDD # 01-080-1197, 00-048-0156 and 00-002-0919) with Miller Index (107) for all the compositions except for the composition ( $x=0.25, y=0.20$ ), for which Miller Index was (114). The crystallite size is calculated using Scherrer's formula.

$$D = \frac{k\lambda}{\beta \cos \theta} \quad (1)$$

Comparison of various structural parameters is given in Table 1. All the samples were with hexagonal structure as primary structure with no sign of any secondary phases. The effect of dopant was also observed by the peak shift toward the higher values of  $2\theta$  angle. The observed variation in both the lattice parameters was due to the difference in ionic radii of  $\text{Sr}^{2+}$  (1.32 Å);  $\text{Ba}^{2+}$  (1.49 Å);  $\text{Fe}^{3+}$  (0.79 Å); and rare earth  $\text{Gd}^{3+}$  (1.07 Å) ions. The doping of bigger size ions caused a slight shift in the X-ray diffraction peaks and expanded lattice which is governed by Vegard's law [10, 11]. Rare earth  $\text{Gd}^{3+}$  ions are expected to replace

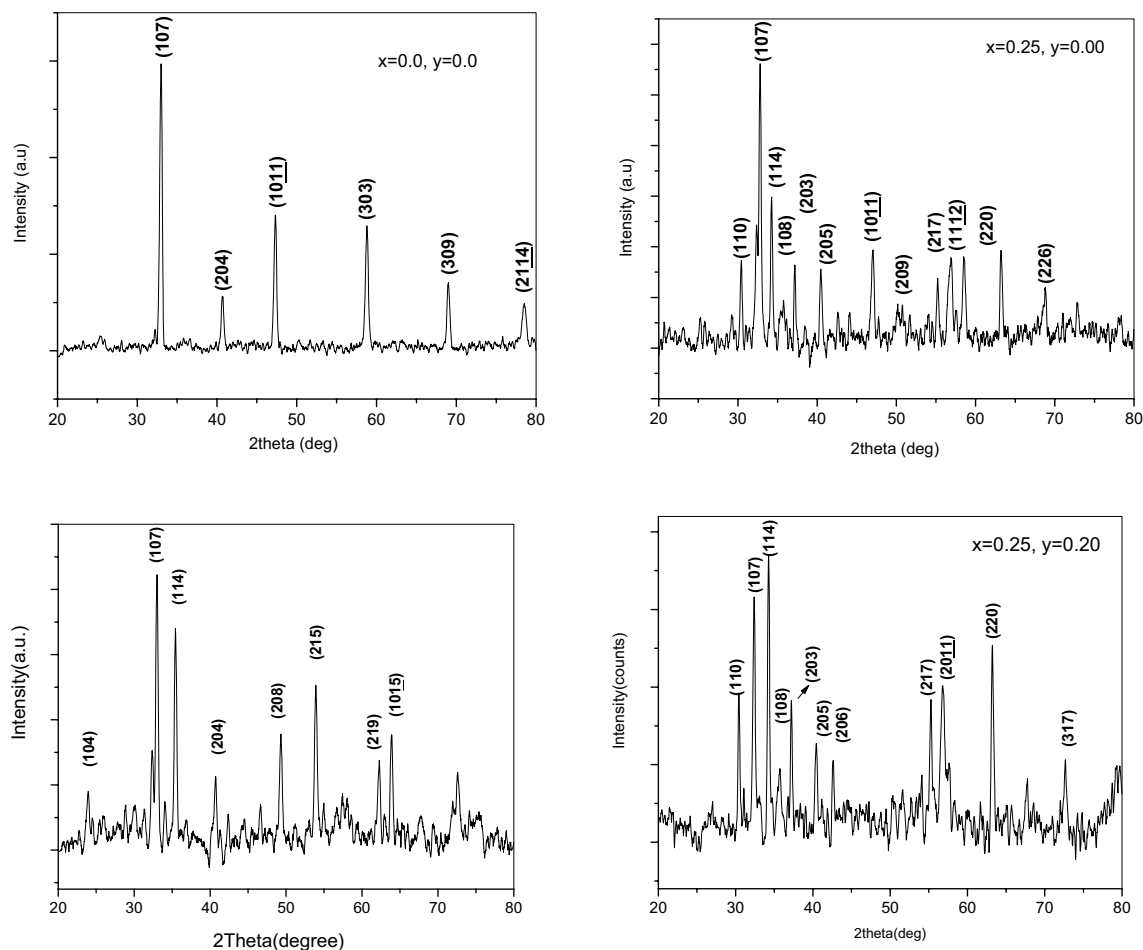


**Fig. 1** XRD pattern of sintered samples with compositions  $\text{Sr}_{1-x}\text{Ba}_x\text{Fe}_{12-y}\text{Gd}_y\text{O}_{19}$  ( $x=0.0, 0.25$  and  $y=0.0, 0.20$ )

**Table 1** Variation in lattice constant “ $a$ ” and “ $c$ ” and crystallite size “ $D$ ” with composition  $\text{Sr}_{1-x}\text{Ba}_x\text{Fe}_{12-y}\text{Gd}_y\text{O}_{19}$  ( $x=0.0, 0.25$  and  $y=0.0, 0.20$ )

Sample name	$D_{\text{max,peak}}$ ( $\pm 1$ nm)	$a$ (Å)	$c$ (Å)
$x=0.00; y=0.00$	56	5.58 (5)	22.74 (2)
$x=0.00; y=0.20$	48	5.58 (6)	22.76 (3)
$x=0.25; y=0.0$	55	5.87 (1)	23.156 (2)
$x=0.25; y=0.20$	84	5.880 (9)	23.076 (2)

$\text{Fe}^{3+}$  sites due to comparable ionic radii and same valence states.

### 3.2 Electrical properties

AC electrical measurements were taken by LCR meter in frequency range 20 Hz–3 MHz at room temperature,

and the DC electrical properties were evaluated as a function of temperature.

### 3.3 Dielectric constant

Performance of dielectric constant at room temperature is given in Fig. 2. The dielectric behavior can be explained based on Maxwell–Wagner two-layer model [10, 11]. It is observed in Fig. 2 that the dielectric constant for all the samples decreased with the increase in frequency due to loss of interfacial polarization. The dielectric constant decreased with increase in frequency of the applied field. The behavior reflects normal behavior of polar dielectric materials, where a polar dielectric material which contributes to the polarization lags the applied field at higher frequencies. The variation of dielectric constant with frequency shows the dispersion in studied samples is Maxwell–Wagner type and is in well agreement with Koop’s phenomenological theory of dielectrics [12, 13]. According to these models, a dielectric structure is supposed to be composed of well-conducting grains, separated by poorly

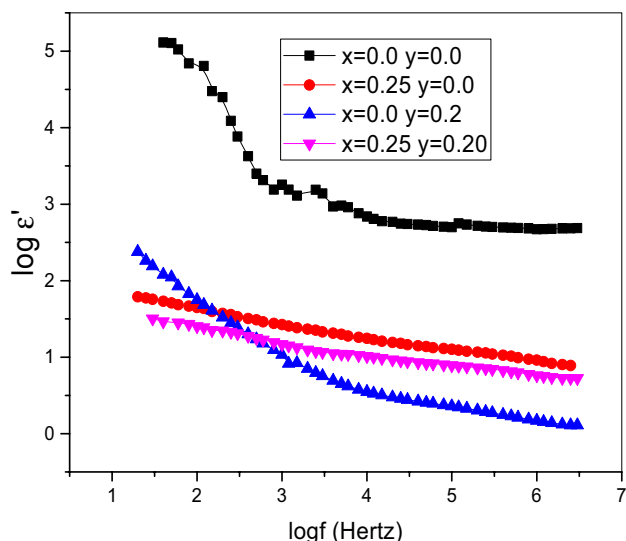


**Fig. 2**  $\epsilon'$  versus  $\log f$  of samples  $Sr_{1-x}Ba_xFe_{12-y}Gd_yO_{19}$  ( $x=0.0, 0.25$  and  $y=0.0, 0.20$ )

conducting grain boundaries. The grain boundaries are formed during sintering process due to superficial reduction or oxidation of crystallites in porous materials due to their direct contact with sintering atmosphere. The polarizations decrease with increasing frequency and then reach a constant value beyond a certain frequency limit where electron hopping cannot follow the changes in an alternating field [12–14]. The dielectric constant of prepared samples can be calculated from usual relations [15].

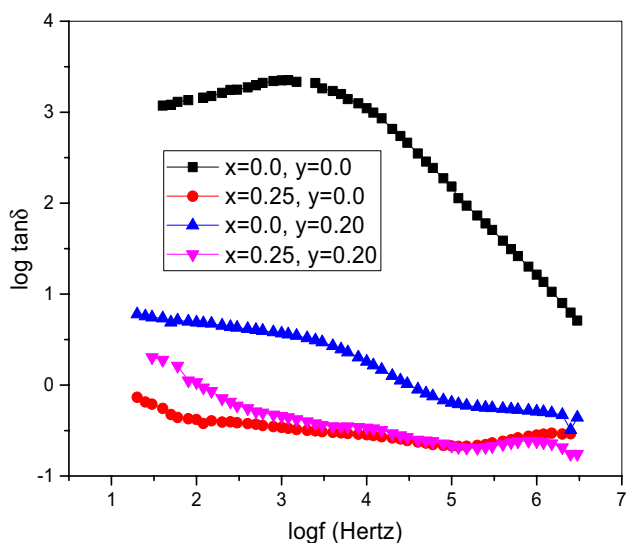


**Fig. 3**  $\tan \delta$  versus  $\log f$  of  $Sr_{1-x}Ba_xFe_{12-y}Gd_yO_{19}$  ( $x=0.0, 0.25$  and  $y=0.0, 0.20$ )

### 3.4 Dielectric loss tangent

Figure 3 shows the dielectric loss tangent which is decreasing with the increase in frequency. The energy loss at higher frequency is given by loss tangent ( $\tan \delta$ ). This usually appears because of lag in change in dipole orientation with respect to the applied electric field. This may be due to defects and the presence of impurities in the material along with the reasons mentioned in the previous section.

### 3.5 AC conductivity

The variation of AC conductivity of hexaferrites as a function of frequency is shown in Fig. 4. AC conductivity is determined by Eq. 2,

$$\sigma_{ac} = \epsilon_o \omega \epsilon' \tan \delta \tag{2}$$

where  $\epsilon_o$  is the permittivity of free space,  $\omega$  is the angular frequency,  $\epsilon'$  is the dielectric constant and  $\tan \delta$  is the dielectric loss. It is observed from graph that  $\sigma_{ac}$  of ferrites increased with the increase in frequency. It is seen that the AC conductivity increases with the increase in frequency of an applied field. Since increase in frequency enhances hopping frequency of charge carriers between  $Fe^{2+}$  and  $Fe^{3+}$  at the octahedral site, the conductivity increases [13, 16]. The sample ( $x=0.25$  and  $y=0.00$ ) showed high conductivity due to dipole polarization. With enhanced frequency hopping of electrons also increased which heightened the conductivity. The increase in conductivity does not mean that the number of charge carriers increases, but only the rate of hopping of charge between the charge carriers,  $Fe^{2+}$  and  $Fe^{3+}$ , increases. The rate of hopping is enhanced once the frequency of the applied field increases, resulting in increase in conductivity and decrease in resistivity

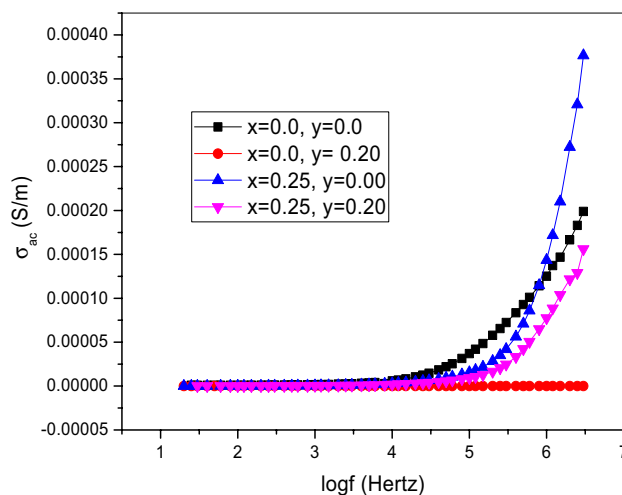


**Fig. 4**  $\sigma_{ac}$  versus  $\log f$  of  $Sr_{1-x}Ba_xFe_{12-y}Gd_yO_{19}$  ( $x=0.0, 0.25$  and  $y=0.0, 0.20$ )

[17]. For compositional effect, it can be shown from Fig. 4 that the value of conductivity decreased with the increase in the concentration of  $\text{Ba}^{2+}$  and  $\text{Gd}^{3+}$ . This is attributed to the greater jump lengths due to higher ionic radii of  $\text{Ba}^{2+}$  as compared to that of  $\text{Sr}^{2+}$  in the first case and to the reduced charge carriers due to replaced  $\text{Fe}^{2+}/\text{Fe}^{3+}$  ions by  $\text{Gd}^{3+}$  in the latter case. Other than compositions, crystallite sizes are also affecting the properties and are responsible for slightly anomalous response [13, 15].

### 3.6 Impedance

Spectra of impedance and real and imaginary parts of impedance were determined at room temperature and are shown in Fig. 5. The frequency range used was 20 Hz–3 MHz. Following Eqs. (3, 4) are used to compute the real and imaginary part of impedance.

$$Z' = Z \cos \theta \quad (3)$$

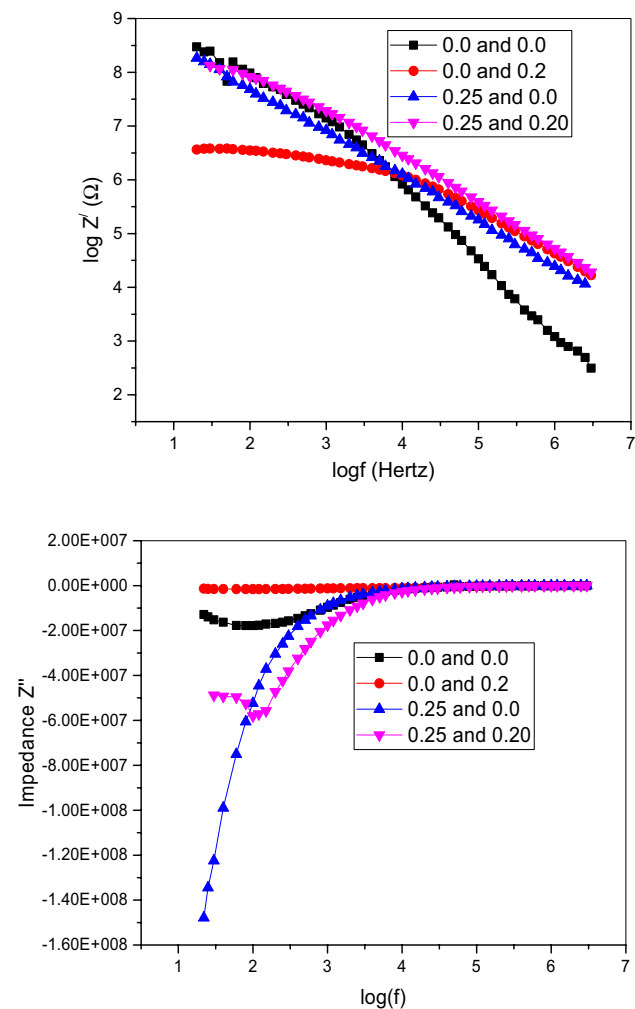


**Fig. 5**  $Z'$  and  $Z''$  versus  $\log f$  of  $\text{Sr}_{1-x}\text{Ba}_x\text{Fe}_{12-y}\text{Gd}_y\text{O}_{19}$  ( $x=0.0, 0.25$  and  $y=0.0, 0.20$ )

$$Z'' = Z \sin \theta \quad (4)$$

where  $Z$  is impedance and ' $\theta$ ' is phase angle. From Fig. 5, it can be observed that real part of impedance ( $Z'$ ) decreased with growing frequency for all samples and reaches a constant value later. This indicates the mobility of polarons. There are three generic relaxation dispersion situations, which may occur for solids while discussing  $Z'$  as a function of frequency: conductive system associated charge carriers, dielectric dispersion usually arising from dipole rotation of lattice entities and the presence of both types of dispersion within measured frequency range. Three different dipolar relaxation processes and an intrinsic conductivity contribution may be involved in this case. Imaginary part of the impedance (Fig. 5) showed a decreasing trend for the all cases. In ferrites, conduction mechanism is due to intra-grain conduction and inter-grain boundaries. The occurrence of relaxation peaks in the imaginary part of complex impedance at low frequencies may be due to the existence of the space-charge relaxation at low frequencies, which is related to the charge carriers in association with the oxygen vacancies. The conductivity is dominated by the short-range hopping of charge carriers [18–20].

Figure 6 shows the Cole–Cole plot (complex impedance plot) for the impedance of all the samples at room temperature. Similar trends could be seen in the literature [8, 14]. The impedance spectroscopy helps in the separation of grain and grain boundary because each of them has different relaxation times, resulting in separate semicircles in complex impedance plane. The spectrum reveals relatively large grain boundary contribution to the total resistivity because close to the grain boundaries, transport properties of the materials are controlled by imperfections, expected to be present in higher concentration than in grains, leading to an additional contribution to the inter-grain (grain boundary) impedance. The internal space charge created at the grain boundaries may lead to a significant increase in the concentration of mobile effects [18, 19].

### 3.7 Temperature-dependent electrical properties

The samples were subjected to temperature increase, and the conduction behavior was observed (Fig. 7). For DC conductivities, it was observed that significant increase was observed after a certain threshold step. This could be attributed to availability of charge carriers and ease in hopping between the sites.

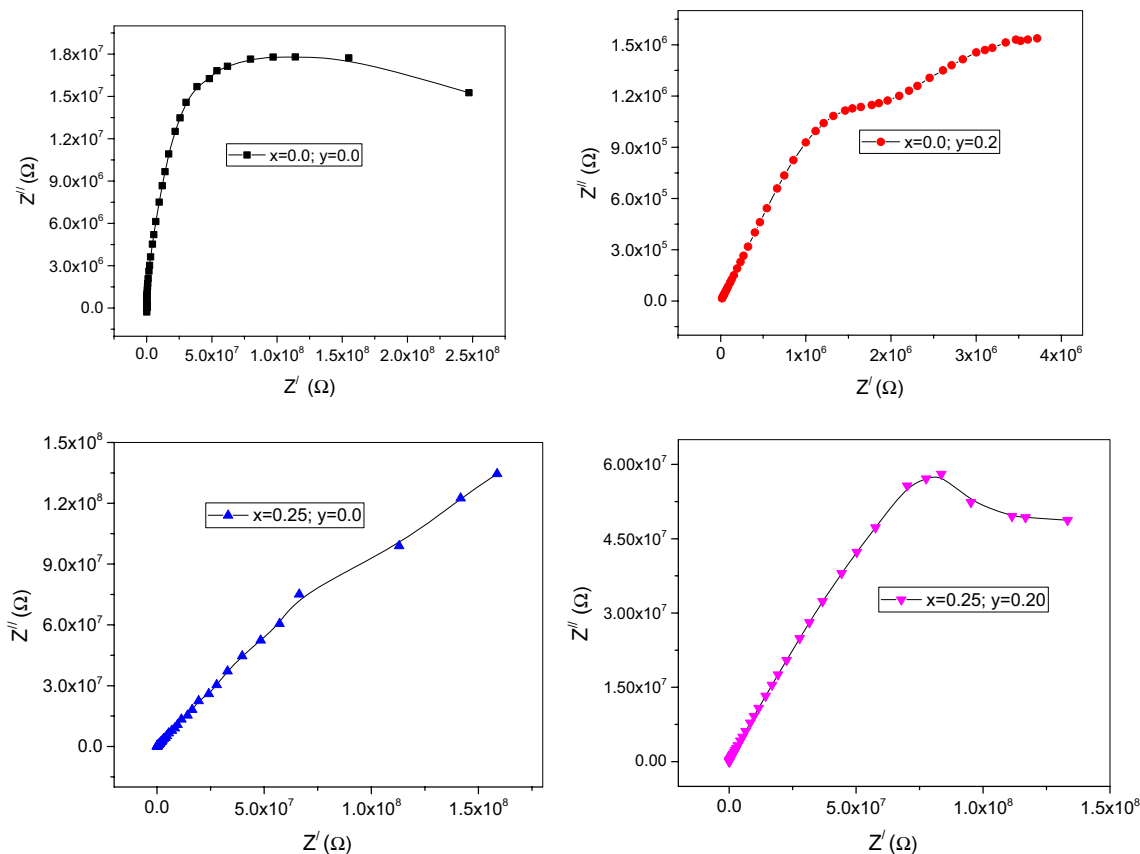


**Fig. 6** Cole–Cole plots for  $Sr_{1-x}Ba_xFe_{12-y}Gd_yO_{19}$  ( $x=0.0, 0.25$  and  $y=0.0, 0.20$ )

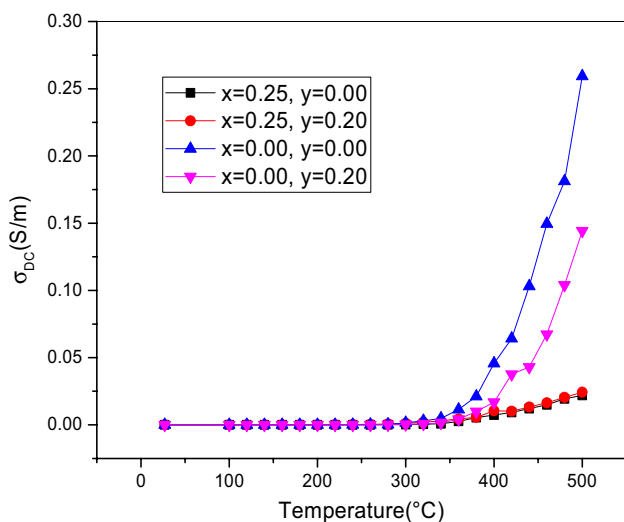


**Fig. 7**  $\sigma_{dc}$  versus temperature of  $Sr_{1-x}Ba_xFe_{12-y}Gd_yO_{19}$  ( $x=0.0, 0.25$  and  $y=0.0, 0.20$ )

### 4 Conclusion

Strontium barium hexaferrites with composition  $Sr_{1-x}Ba_xFe_{12-y}Gd_yO_{19}$  ( $x=0.0, 0.25$  and  $y=0.0, 0.20$ ) were

synthesized by WOS sol–gel method and co-precipitation method. XRD pattern indicates the single-phase hexagonal structure of prepared sample. Crystallite sizes were found to be in range from 55 to 86 nm. In the frequency range of 20 Hz–3 MHz, dielectric constant has higher values at lower frequencies. Dielectric loss tangent decreased due to decrease in  $Fe^{2+}$  ion concentration which is the normal behavior of dielectric properties of hexaferrites. Increase in the concentration of barium as well as that of Gd increased the resistivity and stability of the material. Increased resistivity with doping will be helpful for energy-efficient devices due to reduced eddy current losses. At higher frequencies, AC conductivity increased sharply due to increased hopping rate of ions, relaxation and re-orientation of ions. These properties make hexaferrites suitable for potential application in electronic devices to prevent energy losses. Variation in electrical properties is quite anomalous with composition and frequencies, and this indicates that these materials could be used in a wide variety of applications as per the suitability.

**Acknowledgements** Higher Education Commission (HEC) is acknowledged for providing the financial support during this research.



Assistance of Ms. Uzma Afsar and Ms. Nahall Niazi is also thankfully acknowledged.

## Compliance with ethical standards

**Conflict of interest** The author declares that he has no conflict of interest.

## References

1. Mahmood SH, Awadallah A, Maswadeh Y, Bsoul I (2015) Structural and magnetic properties of Cu-V substituted M-type barium hexaferrites. *Mater Sci Eng* 92:012008
2. Bhatia PG (2016) A study of structural and physical properties of substituted barium hexaferrites. *IJCPS* 5:28–33
3. Rusianto T, Wildan MW, Abraha K, Kusmono (2015) The magnetic and mechanical properties of sintered ceramic magnets  $Sr_xBa_{1-x}Fe_{12}O_{19}$ . *IJET* 15:41–45
4. Cernea M, Negrea RF, Ciuchi IV, Baldisserrri C, Trusca R, Galassi C (2016) Dielectric characterization of  $Ba_xSr_{1-x}Fe_{12}O_{19}$  ( $x=0.05-0.35$ ) ceramics. *Ceram Int* 42:1050–1056
5. Dawarl N, Chitkara M, Sandhu IS, Jolly JS, Malhotra S (2016) Structural, magnetic and dielectric properties of pure and nickel-doped barium nano-hexaferrites synthesized using chemical co-precipitation technique. *Cogent Phys* 3:1208450
6. Bakis Y, Auwal IA, Unal B, Baykal A (2016) Maxwell–Wagner relaxation in grain boundary of  $BaBi_xLa_xFe_{12-3x}O_{19}$  ( $0.0 < x < 0.33$ ) hexaferrites. *Compos B* 99:248–256
7. Wu Q, Yu Z, Hao H, Chu Y, Xie H (2017) The effect of pH value on strontium hexaferrites: microstructure and magnetic properties. *J Mater Sci* 28:12768–12775
8. Nasir S, Asghar G, Malik MA, Anis-ur-Rehman M (2011) Structural, dielectric and electrical properties of zinc doped nickel nanoferrites prepared by simplified sol–gel method. *J Sol-gel Sci Tech* 59:111–116
9. Nasir S, Anis-ur-Rehman M, Malik MA (2011) Structural and dielectric properties of Cr-doped Ni–Zn nanoferrites. *Phys Scr* 83:025602
10. Iqbal MJ, Ashiq MN, Hernandez-Gomez P, Munoz JM (2008) Synthesis, physical, magnetic and electric properties of Al-Ga substituted co-precipitated nanocrystalline strontium hexaferrite. *J Magn Magn Mater* 320:881–886
11. Zhong W, Ding W, Zhang N, Hong J, Yan Q, Du Y (1997) Key step in synthesis of ultrafine  $BaFe_{12}O_{19}$  by sol–gel technique. *J Mater Sci* 168:196–202
12. Batooh KM, Mir FA, El-Sadek MSA, Shahabuddin M, Ahmed N (2013) Extraordinary high dielectric constant, electrical and magnetic properties of ferrite nanoparticles at room temperature. *J Nanopart Res* 15:2067
13. Batooh KM, El-Sadek MSA (2013) Electrical and magnetic transport properties of Ni-Cu-Mg ferrite nanoparticles prepared by sol-gel method. *J Alloys Compd* 566:112–119
14. Batooh KM, Kumar G, Yang Y, Al-Douri Y, Singha M, Jotania RB, Imran A (2017) Structural, morphological and electrical properties of  $Cd^{2+}$  doped  $MgFe_{2-x}O_4$  ferrite nanoparticles. *J Alloys Compd* 726:179–186
15. Asghar G, Anis-ur-Rehman M (2012) Structural, dielectric and magnetic properties of Cr–Zn doped strontium hexa-ferrites for high frequency applications. *J Alloy Compd* 526:85–90
16. Batooh KM (2011) Microstructural and Mössbauer properties of low temperature synthesized Ni-Cd-Al ferrite nanoparticles. *Nanoscale Res Lett* 6:499
17. Batooh KM, Ansari MS (2011) Influence of doping on Dc conductivity of Mn ferrites. In: AIP conference proceedings, vol 1349, no 1, pp 1021–1022
18. Batooh KM, Kumar S, Lee CG (2009) Study of ac impedance spectroscopy of Al doped  $MnFe_{2-2x}Al_{2x}O_4$ . *J Alloys Compd* 480:596–602
19. Batooh KM, Kumar S, Lee CG (2009) Finite size effect and influence of temperature on electrical properties of nanocrystalline Ni-Cd ferrites. *Curr Appl Phys* 9:1072–1078
20. Batooh KM, Kumar S, Lee CG (2009) Influence of Al doping on electrical properties of Ni-Cd nano ferrites. *Curr Appl Phys* 9:826–832

**Publisher's Note** Springer Nature remains neutral with regard to jurisdictional claims in published maps and institutional affiliations.